J. Wind Eng. Ind. Aerodyn. 136 (2015) 127–137

Contents lists available at ScienceDirect

Journal of Wind Engineering and Industrial Aerodynamics

journal homepage: www.elsevier.com/locate/jweia

Moving model analysis of the slipstream and wake of a high-speed train

J.R. Bell [a,*], D. Burton [a], M.C. Thompson [a], A.H. Herbst [b], J. Sheridan [a]

[a] Department of Mechanical and Aerospace Engineering, Monash University, Clayton, Victoria 3800, Australia
[b] Centre of Competence for Aero- and Thermodynamics, Bombardier Transportation, Västeras, Sweden

ARTICLE INFO

Article history:
Received 13 June 2014
Received in revised form
10 September 2014
Accepted 25 September 2014
Available online 29 November 2014

Keywords:
Slipstream
Induced flow
High-speed train aerodynamics
Ground vehicle wake
Transient wake

ABSTRACT

A scaled moving model technique for analysing the slipstream of a high-speed train (HST) with the view of applying this methodology for checking TSI compliance in the design phase of a HST is assessed. Results from experiments are compared to full-scale field test results, and the sensitivity of slipstream to two of the limitations of scaled testing, Reynolds number and the length to height ratio (L/H), is presented. The results captured using this unique methodology provide insight into the transient flow around HSTs.

1. Introduction

The slipstream of a high-speed train (HST) continues to be an important aspect of aerodynamic performance and safe operation. Slipstream is the air flow induced by the train's movement as experienced by a stationary observer. Such flows can be hazardous to waiting commuters at platforms and track-side workers (Pope, 2007). The flows also present the risk of damage to track-side infrastructure. Regulations have been developed in Europe to reduce these risks; for example the European Railway Agency's (ERA) (2008) Technical Specifications for Interoperability (TSI) and the industry norms outlined by the European Committee for Standardization, herein referred to as the European Norms (EN) (CEN European Standard, 2009).

This paper investigates the slipstream of a HST under 'standard operation and configuration', defined here as a single train with one nose and one tail travelling on a straight track over flat ground with no crosswind present. This idealised train is modelled to isolate the slipstream characteristics generated by the train's essential generic geometry in an ideal environment. Under these conditions, the slipstream of a HST has a local peak velocity at the nose passing, a gradual increase in velocity as the boundary layer develops along the length of the train, followed by the largest peak in the near-wake of the vehicle (Baker, 2010; Baker et al., 2001, 2012a,b). These slipstream characteristics correspond to the description by Baker (2010) for flow around a HST having three distinct regions: the nose, boundary layer and wake regions. These general characteristics of a HST's slipstream, illustrated in Fig. 1, are referred to herein as the 'standard slipstream profile' and have been found by a number of researchers in full-scale track-side experiments (Baker, 2010; Baker et al., 2012a; Baker et al. 2012a,b).

Inter-carriage gaps have been found to cause perturbations to this general description as peaks, troughs or waves (Muld et al., 2014a; Pii et al., 2014), however these do not appear to significantly change the rate of increase of the boundary layer thickness. A local tail peak has also been identified in a number of HST slipstream profiles in full-scale experiments (Baker et al., 2012a), scaled experiments (Gilbert et al., 2013), and numerical simulations (Muld et al., 2014a; Hemida et al., 2013), but is not a standard feature and is likely dependent on geometry and measurement position. Both features are included in Fig. 1 as dotted lines to indicate that they are not standard, nor the focus of this research. Further, as the flow around HSTs is highly three dimensional, the slipstream profile as measured by a single streamwise line, as indicated in Fig. 1, is highly sensitive to measurement position, with the shape of the slipstream profile—even the relative magnitudes of the peaks—being susceptible to changes. However, in general the slipstream velocity decreases with increasing height above ground and distances away from train, as shown in full-scale experiments (Sterling et al., 2008) and numerical simulations (Hemida et al., 2013; Huang et al., 2014).

A number of known flow mechanisms can be identified in the wake of a high-speed train: shear layers, von Kármán-type vortex

* Corresponding author.
E-mail address: james.bell@monash.edu (J.R. Bell).

http://dx.doi.org/10.1016/j.jweia.2014.09.007
0167-6105/

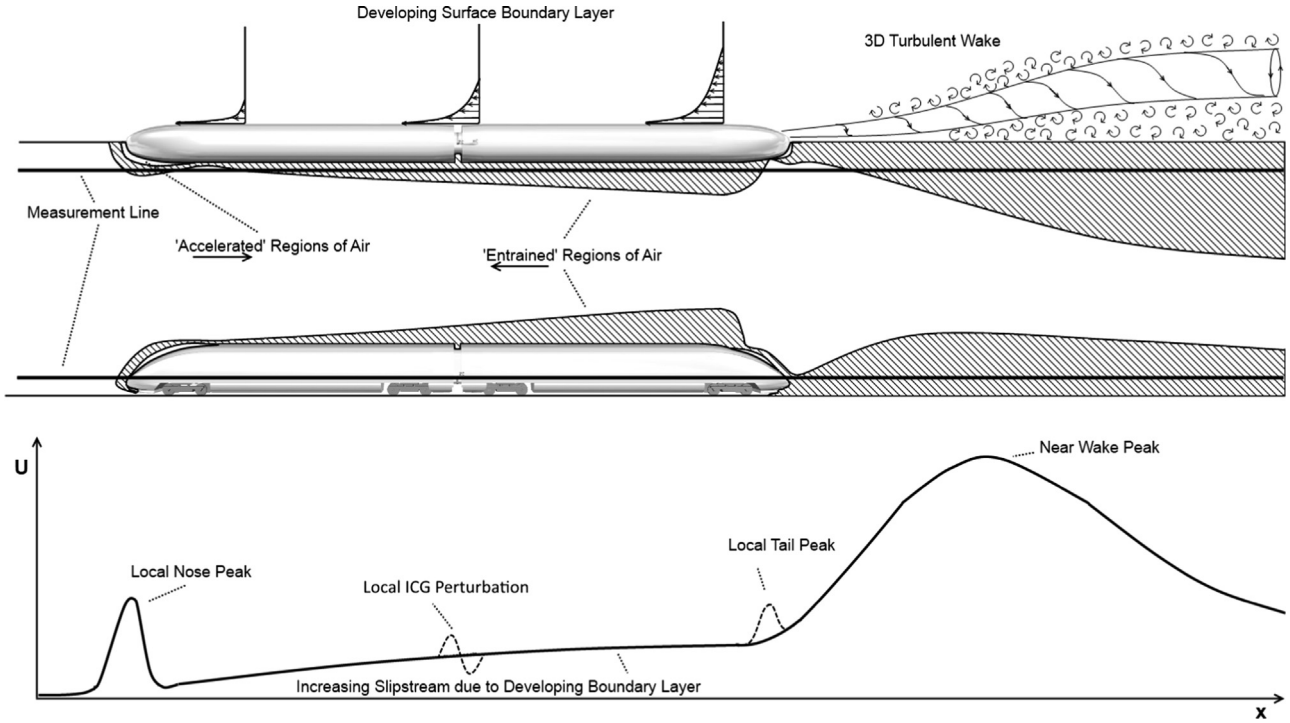

Fig. 1. The slipstream of a high-speed train. The flow induced can travel in two directions: 'Accelerated' flow—travelling opposite to the direction the train is travelling and 'Entrained' flow—travelling with the direction the train is travelling. Accelerated flow is primarily around the head and tail. Increasing thickness of the entrained flow exists over the roof and sides due to the thickening boundary layer. Similarly, a widening region of entrained flow occurs in the wake, expected to be due to the presence of coherent turbulent structures of different scales within the wake. The perturbation in the developing boundary layer—due to the inter-carriage gap—and the local peak at the tail are presented as dotted lines to indicate that they are not found in all HST slipstream profiles.

shedding, separation and recirculation regions and a pair of twin counter-rotating longitudinal vortices (Morel, 1980; Weise et al., 2006; Muld et al., 2012a; Hemida et al., 2013; Huang et al., 2014). The contribution of twin counter-rotating vortices to wake topology has been identified as a particularly important feature in characterising slipstream (Baker, 2010; Weise et al., 2006; Muld et al., 2012a). The counter-rotating vortices are created by the interaction between the down-wash over the roof and tail of the train and the flow around the sides of the train in the transition from a constant cross-section to the end of the tail. These vortices move downwards and outwards due to the mutual induction and interaction with the ground as they progress away from the vehicle (Weise et al., 2006; Muld et al., 2012a; Heine et al., 2013; Schulte-Werning et al., 2001; Yao et al., 2013), with some researchers predicting that they exhibit spanwise oscillations (Muld et al., 2012a; Yao et al., 2013; Schulte-Werning et al., 2003).

The use of a moving model methodology is assessed as a technique for analysing a HST's slipstream and checking for TSI compliance in the design phase. This is performed by comparison to full-scale field test results as well as investigation of the sensitivity of results to the two primary experimental limitations of a moving model methodology: reduced Reynolds number and reduced length to height ratio (L/H). The results obtained are also analysed through ensemble averaging, characterising individual runs, conditional averaging and proper orthogonal decomposition (POD) analysis to provide insight into the transient flow around a HST.

2. Methodology

2.1. Experimental set-up

The experiment was performed at Deutsches Zentrum für Luft- und Raumfahrt (DLR—German Aerospace Centre) Tunnel Simulation Facility (TSG), a moving model facility in Göttingen, Germany. A moving model method has the advantage of measuring slipstream with the same train-measurement probe and train-ground relative motion as full-scale field experiments. The test section, illustrated in Figs. 2 and 3, consisted of 8 m of flat ground, 4 m of which was forwards of the first measurement position. Also included was 6 m of 1/25th scale single track ballast and rail (STBR), 2 m of which was forwards of the first measurement position. Ground configuration is not specified in the EN for scaled model slipstream experiments, however a STBR was required for head pressure pulse investigations in the 2009 EN (CEN European Standard, 2009)—the 2013 EN (CEN European Standard, 2013) revision excluded the rails from this configuration—and crosswind investigations (CEN European Standard, 2010). Thus a STBR ground configuration was modelled in this experiment. A 1/25th scale model of an ICE3—a HST in operation throughout Germany—was used in the experimental work.

Two pairs of light gates (L1 & L2 and L3 & L4 in Fig. 2) were used to determine the model's velocity and acceleration. The model's velocity and acceleration were used to convert the measurements from the time domain to the spatial domain, in which all results are presented. The model's average velocity, U_t, was used to normalise the measured slipstream velocities.

Two modifications aimed at improving the level of detail were made to DLR's ICE3 model, which originally conformed to the EN. The first was to include the wiper geometry at the tail section (omitted at the nose for practical reasons), to ensure that the level of downwash and corresponding strength of the twin counter-rotating vortices was similar to full-scale. The second modification was made to the bogie skirts, coverage was increased to better represent operational ICE3 geometry. This was done to ensure shedding off the exposed region of the bogies, particularly the rearmost bogie, was as realistic as possible.

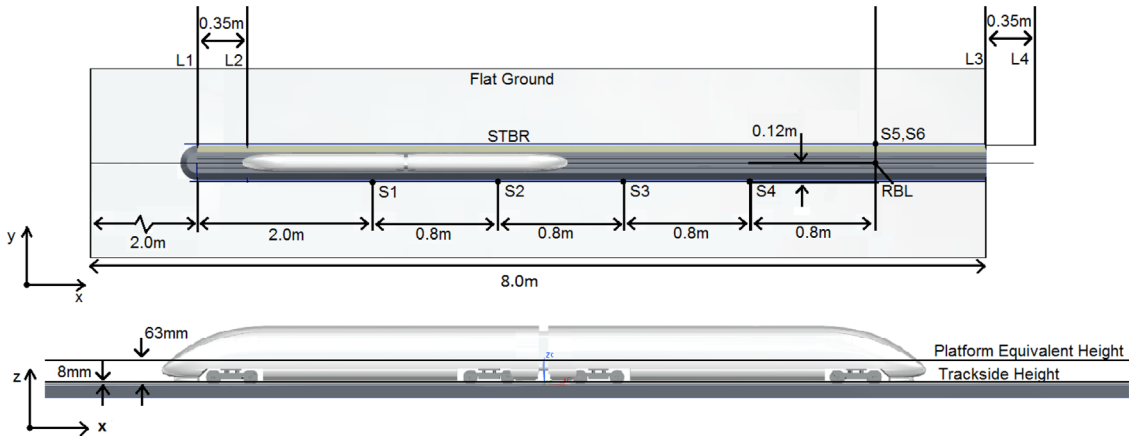

Fig. 2. Moving model experimental set-up at DLR, Göttingen. Black points are slipstream measurement positions, denoted as S1–S6, roof boundary layer rake is denoted as RBL. Light gate pairs L1 & L2 and L3 & L4 are visible forward and rearward of the STBR (dark grey).

Fig. 3. Moving model experimental set-up at DLR, Göttingen.

Three scenarios were tested. The Primary scenario was a 3 car, 2.7 m long model fired at 32 m/s (Re=250,000, width as characteristic length). Operational trains have a length to height ratio (L/H) of 50. The primary configuration of the model had a L/H of 16. The reduced L/H was expected to be a limitation due to the reduction in boundary layer development over the train's surface. Thus the sensitivity of the slipstream results to the L/H and Reynolds number was tested. Both secondary configurations were expected to reduce the level of boundary layer development. The Reduced Length scenario was a 2 car, 2.0 m long model ($L/H=12$) fired at 32 m/s. The Maximum Reynolds number scenario was a 3 car, 2.7 m long model fired at 43 m/s (Re=330,000). Thus sensitivity to Reynolds number over the range of 2.50×10^5–3.3×10^5 was tested, however this is still significantly smaller than the full-scale Reynolds number of 1.7×10^7.

Slipstream results are presented as the equivalent full-scale distance from the tail; full-scale metres (m), with $x=-67.5$ m or $x=-50$ m corresponding to the model nose (2.7 m and 2 m long models respectively) and $x=0$ m corresponding to the tail. Vertical (z) measurements are normalised by the model height (H) of 0.16 m.

2.2. Velocity measurement

Slipstream velocities were measured by hot wire anemometers located as shown in Fig. 2.

The hot wires had a sampling frequency of 50,000 Hz (corresponding spatial resolution of 0.64–0.86 mm), which is larger than the suggested frequency of the EN, and corresponds to a full scale sampling frequency of approximately ≈ 5000 Hz.

Probes S2 and S3 were located at the scaled equivalent to a full-scale track-side measurement position ($y=3$ m, $z=0.2$ m above top of rail, ATOR, European Rail Agency, 2008). The track-side position results are of focus in terms of assessment for TSI slipstream compliance, as they are the direct equivalent to the TSI requirements. These probes were single hot wires mounted perpendicular to the ground plane. This gave the resultant of the u and v components of velocity (horizontal velocity magnitude). This horizontal velocity is denoted herein as U, and corresponds to the velocity used in the TSI slipstream compliance (European Rail Agency, 2008). The vertical component of velocity, w, is not considered as it is proposed that it presents less of a destabilising risk to a standing person because of its orientation (European Rail Agency, 2008).

Probe S4 was located at the scaled equivalent of a full-scale platform measurement position ($y=3$ m, $z=1.58$ m ATOR, European Rail Agency, 2008). This is considered to be a platform equivalent position as no platform was included in this experiment. However, it measures at a similar position relative to the train that the TSI platform position requires ($y=3$ m, $z=1.2$ m above a platform, which at minimum has a height of 0.24 m ATOR, European Rail Agency, 2008), in this case a platform height of 0.38 m ATOR is modelled. Full-scale data compared to below is also measured at this platform equivalent position. Probe S4 was a cross wire, oriented normal to the direction of the flow, thus the u and v components of velocity were calculated separately. The horizontal velocity, U, was subsequently calculated by taking the resultant of these two separate components. It is acknowledged that the cross wire likely measured some portion of the w (vertical) component of velocity, and as a consequence, the U values provided below for S4 are expected to be overestimated.

Probes S2 and S3 had longitudinal spacing of 0.8 m (20 m full-scale), this adhered to the corresponding full-scale specifications: TSI (European Rail Agency, 2008) and the EN (CEN European Standard, 2009) for measurement of the same run with multiple probes, effectively multiplying the number of real runs performed;

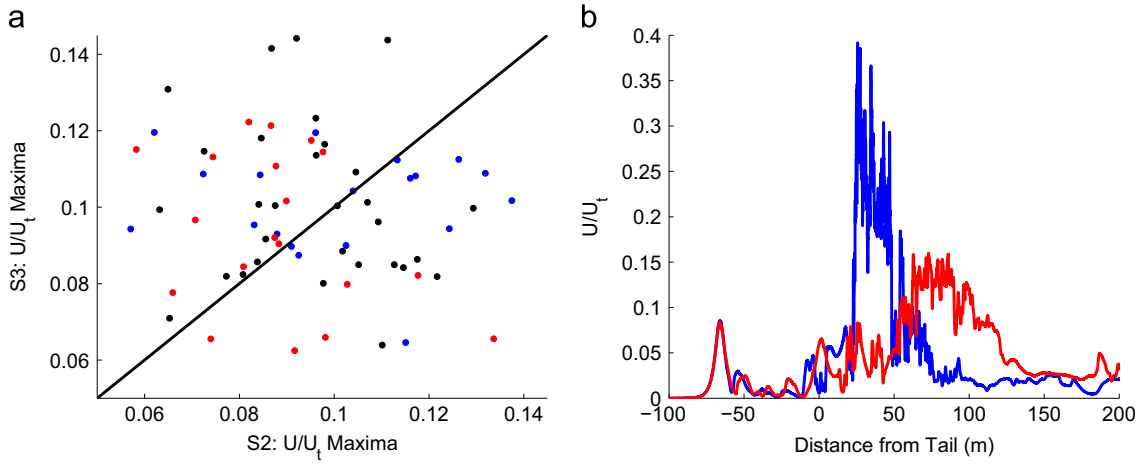

Fig. 4. Correlation of slipstream maxima between S2 and S3 probes for the three moving model scenarios tested. (a) Black line is the 1:1 line, where points would lie if runs were highly correlated. Black squares: Primary maxima, blue squares: Maximum Reynolds maxima, and red squares: Reduced Length maxima. (b) Measurements of an example individual run. Blue: S2 and red: S3. (For interpretation of the references to colour in this figure caption, the reader is referred to the web version of this article.)

'run multiplication'. The correlation between the probes was investigated by comparing the magnitudes of the individual maxima of each filtered run (equivalent to a 1 s moving average). This involved plotting these filtered maxima from probe S2 against the filtered maxima from probe S3. If the maximal magnitude for an individual run measured by probe S2 was the same as S3, the point for that individual line would lie on the 1:1 line, implying 100% positive correlation between the two probes. This method for testing correlation has been established by Baker et al. (2012b) and Baker (2012).

Minimal correlation was found between the two probes' measurements, as seen in Fig. 4. This implies that the large scale turbulent structures (small scale structures are removed with the applied 1 s moving average) believed to be the cause of the maxima are different for the respective S2 and S3 probes.

This allowed the results from probes S2 and S3 to be treated as unique, and justified the use of run multiplication in this experiment. Due to the distance between probes, the minimal correlation and zero ambient wind, interference effects between the hot wires were assumed to be negligible. This resulted in 60 effective runs processed for the Primary scenario, and 40 for the Reduced Length and Maximum Reynolds scenarios at track-side position, and 30, 20 and 20 at platform position respectively.

2.3. Gust analysis

Gust analysis in a scaled equivalent to that outlined in the TSI and EN for slipstream holmologation of a HST (European Rail Agency, 2008; CEN European Standard, 2009) was performed in this experiment. The ability to do such analysis directly is the primary benefit of a moving model method. In the TSI regulations, a HST's slipstream performance is assessed using a single value, herein referred to as the 'TSI value', which is the 95% confidence interval for a 1 s gust. This is based on the mean and standard deviation of a data set comprising the maxima from each filtered (1 s moving average) individual run, as calculated by the following equation:

$$U_{2\sigma} = \overline{U} + 2\sigma. \tag{1}$$

In this experiment, the velocity measured was first converted from the time domain to the spatial domain utilising the scaled model trains speed, U_t. In full-scale field experiments, a 1 s moving average in the time domain is equivalent to an 83.3 m moving average in the spatial domain, as the train is travelling 83.3 m/s (300 km/h). To ensure an equivalent moving average in this scaled experiment, the moving average applied was a 3.33 m (83.3/25) spatial moving average. This was to ensure that the same size flow structures were analysed in the scaled experiment compared to the full scale, all other things being equal. This method of converting to the spatial domain utilising the model train speed incorporates both the length and velocity scales, which is a higher level of detail to that suggested in the EN for scaled testing (CEN European Standard, 2009), which only accounts for length scale.

2.4. Roof boundary layer

The roof boundary layer was measured for each scenario using a boundary layer rake with five pitot tubes (z=0.025, 0.047, 0.072, 0.097 and 0.120H above the roof) and one static tube (z=0.195H above roof). It was assumed that no vertical static pressure gradient existed above the flat roof of the model, thus the dynamic pressure at each point was obtained by deducting the static pressure measured from the respective total pressures measured by the pitot tubes.

Ensemble averages calculated from the individual runs, which each had a 1000 Hz low-pass filter applied, at each measurement height are presented in Fig. 5a. Examples of the boundary layer velocity profiles used to calculate the momentum thickness along the train's length are presented in Fig. 5b, where velocity was converted to the train-fixed frame of reference to present the ground boundary layer in its more common form, this was done using the following equation:

$$U_{TF} = 1 - \frac{U_{GF}}{U_t}, \tag{2}$$

where U_{TF} is the velocity in the train-fixed frame-of-reference, U_{GF} is the velocity in the ground-fixed frame-of-reference, as measured in the experiment, and U_t is the velocity of the train.

The increasing thickness of the boundary layer is visible in Fig. 5a and b.

The boundary layer over a HST has been shown to be highly three dimensional (Baker, 2010), with the side boundary layer being sensitive to distance above the ground. Thus, the roof boundary layer was measured and analysed as a 2D boundary layer for simplicity, as previous researchers have done (Baker, 2010; Muld et al., 2014b). The resulting momentum thickness development profiles (Fig. 6) are calculated using

$$\theta(x) = \int_0^\infty \frac{U}{U_\infty}\left(1 - \frac{U}{U_\infty}\right) dy, \tag{3}$$

show that the increased Reynolds number did not significantly reduce the momentum thickness, the reduced length, however, resulted in a thinner boundary layer at the tail. The influence of the nose of the train is identifiable up to the first inter-carriage gap (ICG1), where a

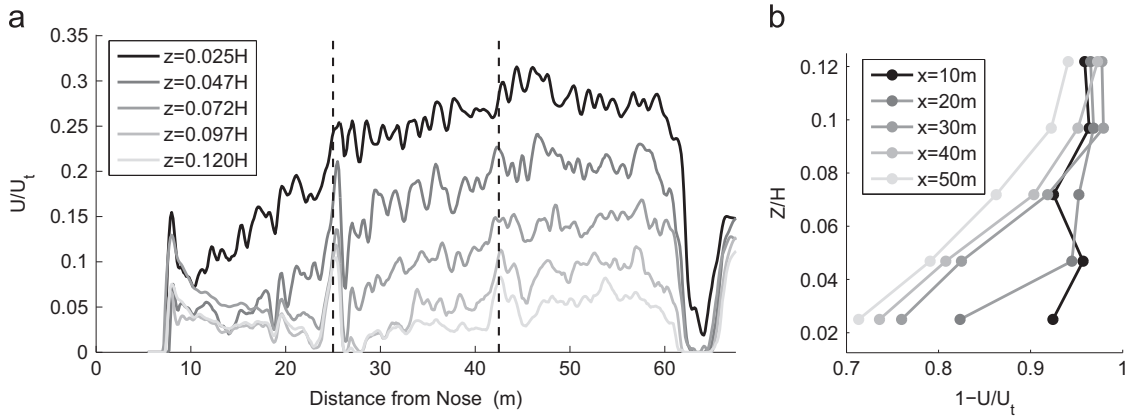

Fig. 5. (a) Ensemble averages from measurements at $z=0.025$, 0.047, 0.072, 0.097 and 0.120H above the roof. (b) Velocity profiles at $x=10$, 20, 30, 40 and 50 m from the nose.

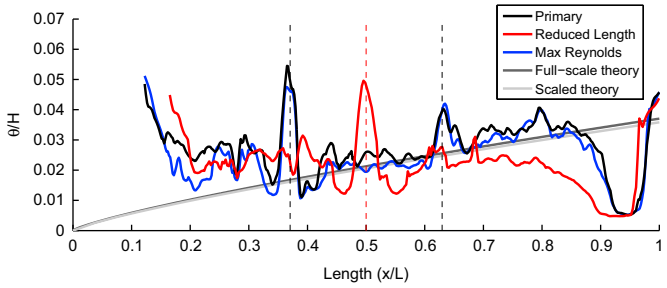

Fig. 6. Normalised momentum thickness at $y=0$ over the roof of the model. Black: Primary, red: Reduced Length, and blue: Maximum Reynolds scenarios. Black dotted lines: ICG1 & ICG2 and red dotted line: ICG1 for Reduced Length scenario. Dark grey: Full scale—flat plate theory and light Grey: 1:25 scale—flat plate theory. (For interpretation of the references to colour in this figure caption, the reader is referred to the web version of this article.)

sharp increase is visible in all three scenarios ($x=25$ m). After ICG1, the gradual increase can be seen along the length of the model.

The influence of the second inter-carriage gap (ICG2) is visible ($x=42.5$ m) in the Primary and Maximum Reynolds scenarios, however aside from the peaks at this location, the overall influence on the development appears minimal. This suggests the ICG has little influence on global boundary layer development. This tendency for the ICG to be visible in the boundary layer profile, but have a negligible effect on the overall development, can also be seen in the numerical research by Muld et al. (2014b).

Also included in Fig. 6 is the momentum thickness (see Eq. (3)) development for a turbulent boundary layer based on the empirical formula provided in Eq. (4) (Munson et al., 2006) for two cases:

$$\theta(x) = 0.0360\left(\frac{\nu}{U_\infty}\right)^{1/5} x^{4/5}. \tag{4}$$

The first case aims to estimate the development over the scaled model using a flat plate of length 2.7m - the same length of the scaled model – with a freestream velocity of 32m/s. The second case aims to estimate the development over a full-scaled model using a flat plate of length 200 m with a freestream velocity of 83.3 m/s. This approach was taken by Muld et al. (2014b).

The x-axis in Fig. 6 is the relative position along the roof (x/L) which uses the total length (L) of each specific scenario plotted to normalise the data. This enables a direct comparison of momentum thickness at the tail, which is the focus in this case.

These results highlight the effect the Reynolds number has on boundary layer thickness, where even though the full scale case is 200 m, two orders of magnitude larger than the scaled, thus providing the boundary layer a longer time to develop, the significant difference in Reynolds number (scaled Re: 5.92×10^6, full scaled Re: 1.14×10^9, using model length as the characteristic length) results in very similar momentum thickness development over the model, and most importantly the thickness at the tail, which is expected to have the greatest influence on the near-wake.

The estimated momentum thickness at the tail using the empirical formula for a flat plate also compare reasonably well with the scaled experimental Primary and Maximum Reynolds scenario results.

If we assume that the flat plate formula is also a good estimation for momentum thickness development over the full scale train, then it is likely that the reduced L/H ratio of the scaled models is not necessarily a significant experimental limitation. This is because the reduced Reynolds number of the experiments will compensate for the reduced L/H ratio compared to full scale.

The Reduced Length scenario reaches a momentum thickness of 0.02 before the effects of the tail are visible, where both the Primary and Maximum Reynolds reach 0.035. However, the effect of the tail results in all three scenarios having almost identical profiles at the end of the train.

2.5. Full-scale field experiment

The full-scale results presented are from field tests undertaken in Spain as part of Work Package 5 of the AeroTRAIN Project. These results are from an 8 car, 200.3 m long Siemens Velaro S-103 high-speed train, and are a subset of data presented in Baker et al. (2012a,b) and Baker (2012). The external geometry of the S-103 is considered the same as the ICE3 geometry of the scaled moving model used in this experiment.

Induced velocity was measured by a number of ultra-sonic anemometers with a sample frequency of 265 Hz, corresponding to a spatial resolution of 0.3 m. This is larger than the 100 Hz minimum required by the TSI and EN regulations.

For the ensemble averages calculated and presented, 20 of the lowest ambient wind runs with train speeds above 70 m/s were selected to be processed. For gust analysis, the 20 lowest ambient wind runs were processed, while runs that satisfy the TSI criteria: $V_{\max}(83.3\text{ m/s}) \pm 10\%$, ambient wind less than 2 m/s (European Rail Agency, 2008) were also processed and are presented separately for comparison.

3. Results

3.1. The flow around high-speed trains

The results in this section provide insight into the flow around a high-speed train and how the method of a moving model

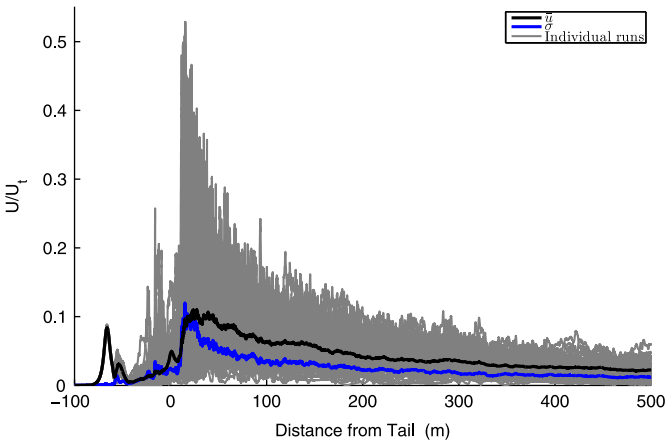

Fig. 7. The flow around a high-speed train, as measured and represented by moving model methodology. Black: ensemble average, blue: ensemble standard deviation, and grey: 60 individual runs. Results are taken from the Primary scenario at track-side measurement position. (For interpretation of the references to colour in this figure caption, the reader is referred to the web version of this article.)

captures and therefore represents these phenomena. The individual runs, ensemble average and standard deviation for the Primary scenario measured at the track-side position, are presented in Fig. 7.

The 'standard slipstream profile' is clearly visible in the ensemble average, with a peak velocity at the nose passing, a gradual increase in velocity as the boundary layer develops along the length of the train, followed by the largest peak in the near-wake of the vehicle.

The ensemble standard deviation exhibits very low deviation at the nose peak, illustrating its highly repeatable nature, this also occurs at the tail of the train, albeit to a lesser extent, suggesting some variation run to run of the tail peak. The near-wake experiences the highest deviation, with a peak magnitude similar to the near-wake peak in the ensemble average, however the standard deviation peak dissipates much earlier.

The run-to-run variation of the individual slipstream profile is evident in Fig. 7 in both the individual runs and ensemble standard deviation. The difference between the individual runs and the ensemble average highlights the shortcomings of using an ensemble average to describe a transient feature. Fig. 8a–c is the enlarged sections of the near-wake displayed in Fig. 7, with selected individual runs plotted to better represent the significant differences between runs.

In Fig. 8, the five selected runs display the variation in location of the near-wake peak, ranging from 10 m to 60 m from the tail. The peak magnitude depends on the location, which is largest at 15 m from the tail, and decreases thereafter. Each individual run's peak contributes to a portion of the upper limit of all runs visible in Fig. 7.

It is proposed that the difference in individual runs are a result of capturing different phases of a transient wake. Previous researchers have identified a pair of streamwise, counter-rotating vortices in the near-wake of high-speed trains (Baker, 2010; Morel, 1980; Weise et al., 2006). The authors of this paper have also previously identified these structures in time-averaged flow around a high-speed train with dominant frequencies of St: 0.18, and linked these to the near-wake peak in slipstream profiles in wind tunnel experiments (Bell et al., 2014). Research in the transient wake has suggested that this vortex pair oscillates in the span-wise direction (Muld et al., 2012a; Schulte-Werning et al., 2003), this is further explored in Sections 3.2 and 3.3.

The relationship between peak location and magnitude does not explain the breadth in magnitude of individual profiles at a

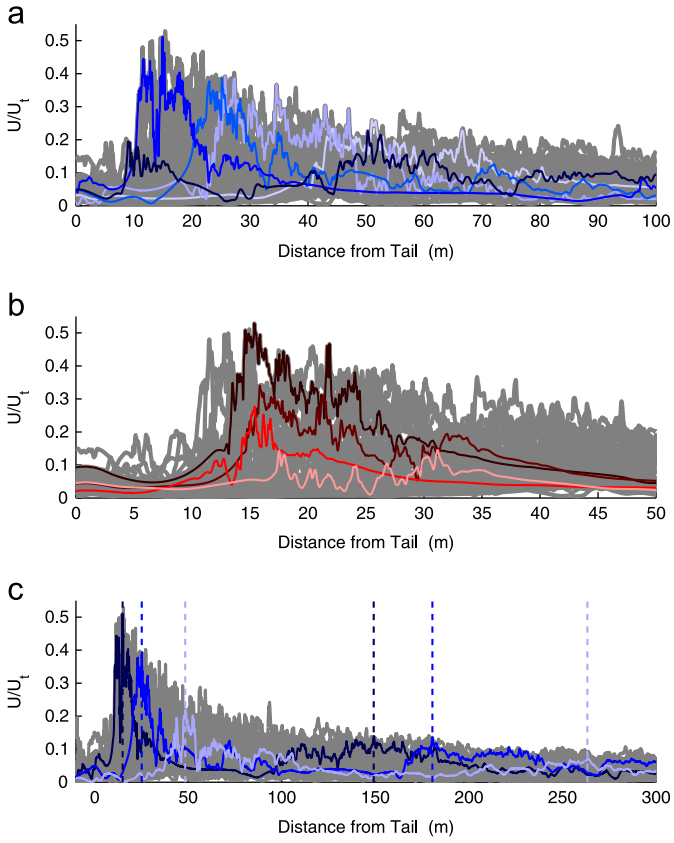

Fig. 8. Selected individual runs taken with the Primary scenario at track-side measurement position. (a) The variation in location of near-wake peak. (b) The variation in magnitude of near-wake peak. (c) The presence of primary and secondary peaks in the wake.

single position, visible in Fig. 7. This is clearly presented in Fig. 8b which shows a number of peaks in the near-wake at approximately the same position ($x=15$ m), yet having different magnitudes (0.15–0.51). This is possibly due to the difference in coherence of the vortices between runs.

A periodic wake is also indicated by the selected runs displayed in Fig. 8c, where three runs have clear secondary peaks in the far wake. The distance between the primary and secondary peaks is dependant on the primary peak's location, it increases further the primary peak is from the tail (135 m, 155 m and 215 m with primary peaks at 15 m, 25 m and 50 m respectively). One would expect this as the wake is stretching as it is dragged behind the train.

The characteristics displayed above are consistent across the other moving model scenarios tested at both track-side and platform height, as well as in full-scale field results analysed.

3.2. Conditional averages

In an attempt to explain the transient wake evident in Figs. 7 and 8 in Section 3.1, conditional averaging was applied to the 60 individual Primary scenario runs at track-side height. The condition was the average slipstream value between 10 m and 100 m from the tail as this was the region of the near-wake peak and highest variation run to run, beyond which the slipstream velocities of the individual runs converge. Ensemble averages were calculated from 10 runs with the highest (Max), medium (Mid) and lowest (Min) average slipstream velocity over this range.

A comparison of ensemble averages for each case is presented in Fig. 9. There are clear differences between the three cases, most notably in the near-wake peak magnitude and location. These

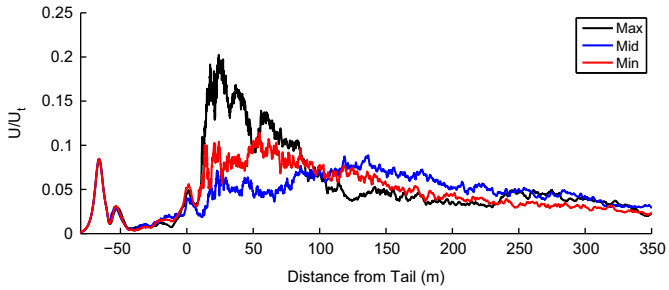

Fig. 9. Conditional averaging showing three cases: Maximum (black), Mid (red) and Minimum (blue) ensemble averages are presented. Ensemble averages presented are calculated from 10 runs with the highest (Max), medium (Mid) and lowest (Min) average value over 10–100 m range in the near-wake. (For interpretation of the references to colour in this figure caption, the reader is referred to the web version of this article.)

differences are thought to be due to the measurement probe capturing the periodic flow of the wake at different phases as it is dragged behind the train past the probe. If the peaks are due to the presence of twin counter-rotating vortices passing the measurement probe (Baker, 2010; Weise et al., 2006; Morel, 1980), that oscillate horizontally (Muld et al., 2012a; Schulte-Werning et al., 2003), then one would expect three primary phases in the flow: capturing the peak as the closest of the vortices moves towards the measurement probe, capturing the trough as the vortex moves away from the measurement probe, and capturing the equilibrium phase, by oscillating towards either side. Therefore it is proposed that these three phases respectively correspond to the Max, Min and Mid cases established in Fig. 9. This hypothesis also explains the nature of the Min case having a peak further in the wake, attributing this to a vortex that oscillates towards the measurement probe far later in the wake albeit with lower slipstream magnitude. The medium level peak in the Mid case could be attributed to strong but smaller scale turbulent structures present in the very near-wake that dissipate quickly.

Conditional averaging was also performed using the peak location as the condition. This resulted in very similar results to those presented above.

The validity of performing conditional averaging is established in Fig. 10, where the respective ensemble average is an acceptable representation of the corresponding individual runs, and distinct differences between the groups of the individual runs are evident.

3.3. Proper orthogonal decomposition

Proper orthogonal decomposition (POD) was performed in an attempt to gain further insight into the run–run variation in the near-wake. POD has been used extensively to provide insight into coherent structures in fluid dynamic problems (Perrin et al., 2007; Graftieaux et al., 2001; Muld et al., 2012b) and more recently specifically in the wake of HST's (Muld et al., 2012a). POD applied to data acquired in this experiment is somewhat novel, however, due to the frame of reference between the measurement equipment and model. The result is that individual runs are considered as 'snapshots' used in the POD process. In this case there is no time correlation between runs, therefore frequency analysis of modes cannot be performed.

Each individual run in reality is not a true 'snapshot' as the flow is expected to change during the time the model moves past the measurement probe. The expected range of dominant frequencies within the wake is St: 0.1–0.2 from the literature (Muld et al., 2012a; Schulte-Werning et al., 2003; Bell et al., 2014) which corresponds to frequencies of 10–32 Hz at U_t=32 m/s. The model would travel between 1.45 and 3.45 m (U_t=32 m/s) for one period of these expected frequencies, which when compared to the scaled

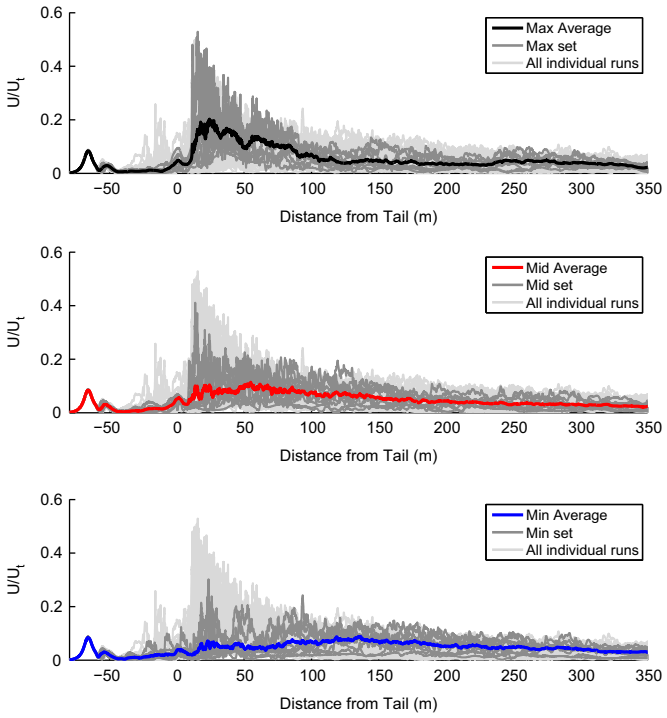

Fig. 10. The set of individual runs used to create the three conditional ensemble averages; Max, Min and Mid, presented in Fig. 9, compared to all individual runs.

size of the near-wake variation (3 m) is not ideal. Thus the wake is likely changing to some extent during the measurement of each run, as such, the results from POD are proposed simply to highlight the variability and recreate a set of simplified run profiles.

The percentage of total energy of the fluctuating motion (the energy of the time-averaged is not considered) is presented in Fig. 11. Modes 1 and 2 are shown to share a large portion of the energy having 19% and 16% respectively. The third and fourth modes have a similar proportion of 9% and 8%, with a clear drop in energy for higher modes.

The time-averaged (Mode 0) and the first four fluctuating modes (Modes 1–4) are presented in Fig. 12. The 'range' of each fluctuating mode from the 60 individual runs from the Primary scenario, track-side measurements are presented. A 'max' and 'min' case for each mode was calculated from the mean plus or minus two standard deviations of the mode coefficients from the data set of 60.

It is clear that the first mode corresponds to a sharp major near-wake peak close to tail which are evident in a number of individual runs. A second peak further in the wake is also evident in the first mode. The second mode shows a broader lower peak further from the tail with no secondary peak, again a characteristic that is visible in a number of individual run profiles. The third and fourth modes show lower magnitude multiple peaks which suggest that they have a less significant influence on the overall profile.

Reconstruction of a number of potential profiles was performed considering the range of the first two mode coefficients from the 60 runs, as well as the correlation of mode coefficients between these two modes. The correlation coefficient between the first two modes was found to be negligible at 2.1×10^{-4}. Thus four potential profiles were reconstructed using combinations of the 'max' (mean plus two standard deviations) and 'min' (mean minus two standard deviation) mode coefficients of the first two modes. This is presented in Fig. 13. The range of the four potential profiles shares a similar envelope to the raw individual runs, with only the maxima of the near-wake peak not being well represented. This

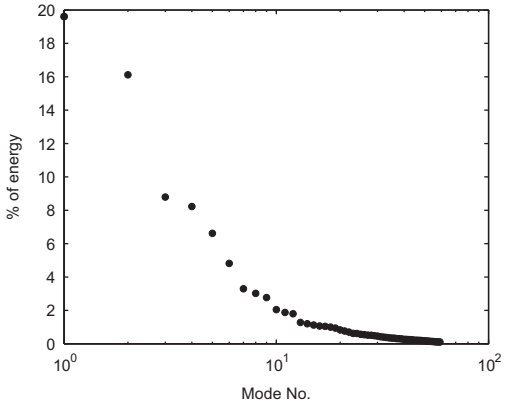

Fig. 11. Percentage of the total energy of the fluctuating motion for modes 1–60.

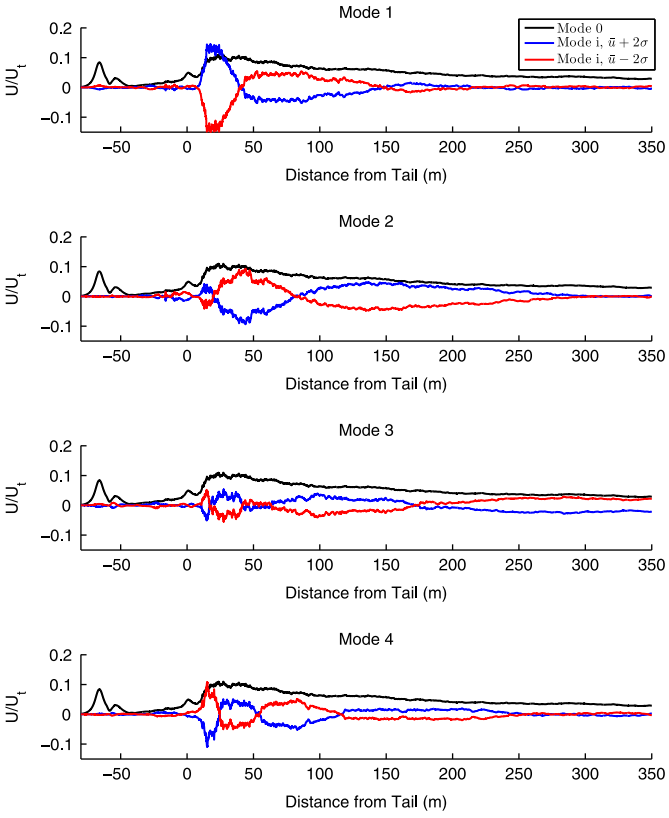

Fig. 12. Modes 1–4 are shown with the 95% confidence interval of mode coefficient range. Black: time-averaged mode—0, blue: mean$+2\sigma$ of corresponding mode, red: mean-2σ of corresponding mode. (For interpretation of the references to colour in this figure caption, the reader is referred to the web version of this article.)

perhaps could be achieved by including modes beyond the first two. The validity of the reconstructed potential runs is strengthened by comparison to Fig. 8 where raw individual runs can be seen with the same characteristics. These results indicate that the run–run variation is due to the variation of two dominant coherent structures in the near-wake.

Although reconstruction cannot be made in the time domain, i.e. how each potential profile transitions to the next, intuitively one can imagine the main peak propagating further into the wake behind the tail eventually leading to the secondary peak visible in profile 1 and the cycle repeating itself. The order of this would be: profile 1 (mode 1: max, mode 2: max), profile 2 (mode 1: max, mode 2: min), profile 3 (mode 1: min, mode 2: min), and profile 4 (mode 1: min, mode 2: max). In this simplistic model, the two

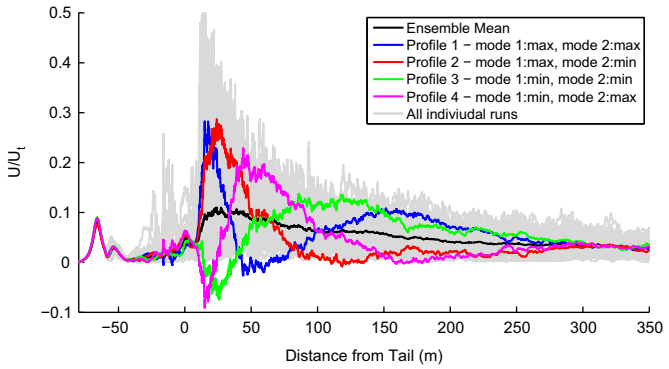

Fig. 13. Potential profiles' reconstructions using combinations of the mean (Mode 0), and two primary fluctuating modes: Mode 1 and Mode 2.

modes have the same frequency but are out of phase, thus no correlation was found.

3.4. Ensemble averages

The ensemble averages of the three moving model scenarios are compared in this section to gain insight into the sensitivity of the results from a moving model method to Reynolds number and model length. These results are further compared to full-scale results to determine the validity of any findings and accuracy of the method.

The 'standard slipstream profile' is clearly visible in the moving model ensemble averages at track-side and platform equivalent heights presented in Fig. 14a and c respectively.

At track-side height, the minimal difference between the Primary and Maximum Reynolds profiles indicates Reynolds number insensitivity over the limited range tested (250,000–330,000). The Reduced Length scenario shows a larger (magnitude of 0.15) and wider peak in the near-wake, compared to the Primary and Maximum Reynolds peak magnitudes (0.11 and 0.125 respectively). This is proposed to be due to the difference in boundary layer development (Fig. 6). A possible explanation for the increased slipstream peak is that the reduced boundary layer at the tail corresponding to a higher frequency oscillation of the vortices, as hypothesised by Muld et al. (2014b), is expected to be due to a thinner effective characteristic width used to calculate the Strouhal number due to a smaller displacement thickness. This could lead to an increased measurement of peaks given more frequent peaks with no change in the moving average. Further, a smaller boundary layer could also allow a stronger wake and therefore larger near-wake peak.

The full-scale ensemble average at track-side position has a lower and flatter slipstream peak in the near-wake compared to the moving model results. However, the filtered ensembles (respective smooth lines) of all moving model scenarios compare very well to full-scale. This suggests that differences in the magnitude of the peaks in the unfiltered profiles are small enough that they may not necessarily influence a gust type analysis.

Features observed at track-side height are not apparent at platform equivalent height (Fig. 14c and d). The moving model scenarios do not compare well to each other, with none comparing well to the full-scale results. This could be attributed to the reduced individual runs used, with only one probe measuring at platform height, run multiplication could not be utilised, thus the ensemble averages were based on half the number of runs than the track-side ensemble averages.

The overall profile of the platform position, Primary ensemble average is similar to the full-scale, with a similar shaped tail peak and a broad and distant (100 m from the tail) near-wake peak.

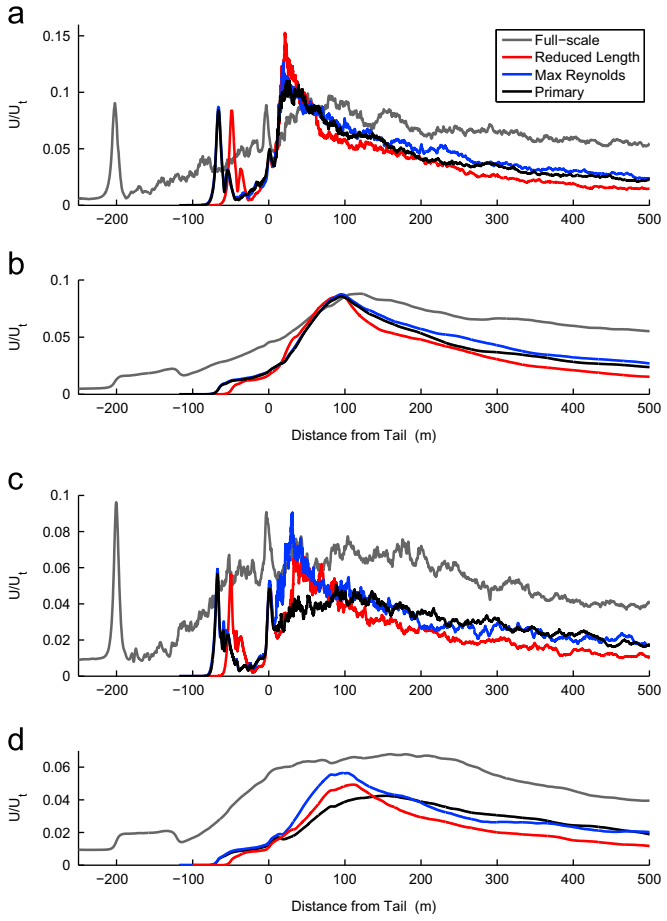

Fig. 14. Track-side position: (a) ensemble averages and (b) equivalent 1 s moving average. Platform position: (c) ensemble averages and (d) equivalent 1 s moving average.

However, the slipstream velocity is consistently less than the full-scale. The Maximum Reynolds scenario has a near-wake peak magnitude similar to full-scale (0.09), however with a narrower and closer peak (30 m from the tail). The Reduced Length is in between the Primary and Maximum Reynolds scenarios, in both near-wake peak magnitude and distance from the tail. The moving average profiles also do not compare well to full-scale at this platform equivalent height, as the differences in the raw profiles are too profound.

Close inspection of the moving model nose peaks identifies a double peak that is not apparent in the full-scale results. This is due to the forward facing probe arms used in the scaled experiments, which prohibit the measurement of reversed flow (accelerated flow around the trains nose) that is able to be measured in full-scale by the vertically mounted ultra-sonic anemometers.

It is possible that greater boundary layer development occurs in full-scale, as the L/H is 50, compared to the scaled models of 16. This difference in boundary layer thickness and the resulting influence on the near-wake potentially explains the difference between the moving-model and full-scale results.

The ideal nature of these moving model experiments (with zero ambient wind) also provides a possible explanation for the stronger peaks compared to full-scale. This difference in ambient wind is visible in Fig. 14, where the upstream slipstream velocity is 0.01 at both heights in the full-scale results, whilst being 0 for all moving model scenarios.

It is proposed that the platform measurement position—at a greater distance from the ground—is on the outer edge of the pair of counter-rotating vortices expected to be responsible for the near-wake peak. This explains the generally lower slipstream values at higher measurement positions (Baker et al., 2012a). Thus any differences within the wake as a result of the moving model scenarios are more easily observed as the dominant flow feature is measured less directly.

Further, both the high Reynolds number and the non-ideal conditions at full-scale are expected to reduce the coherence of any turbulent structures that exist in the ideal conditions and lower Reynolds number flow of the scaled moving model experiment. This reduced coherence should result in a more spread out, 'noisier' wake structure. This explains the full-scale track-side ensemble average having a broader and lower peak magnitude that takes significantly longer to dissipate than in the moving model. This hypothesis also explains why the full-scale platform ensemble average has a broader and higher peak magnitude than the moving model.

Acknowledging that the coherence at full-scale is likely to be reduced, the overall agreement in ensemble average profiles suggests that the moving model does represent and measure the flow around a high-speed train. It does this, however, in a cleaner, more ideal manner.

3.5. Ensemble standard deviation

As highlighted in Section 3.1, the ensemble average does not represent the individual runs well. Therefore the ensemble standard deviations of the moving model scenarios and full-scale experiment are presented separately in this section.

The track-side ensemble standard deviations show no discernible difference between the various moving model scenarios (Fig. 15a) but all scenarios overestimate the standard deviation compared to the full-scale results.

The platform ensemble standard deviations show that there are differences between the three moving model scenarios (Fig. 15b), with the Maximum Reynolds having the highest in the near-wake peak, followed by the Reduced Length, and then the Primary scenario. The full-scale is most similar to the Primary scenario but only in the near-wake peak.

As suggested in Section 3.4, the reduced coherence in the full-scale wake, which causes the 'noiser' wake structure, could also be the cause of the differences in the standard deviation. Assuming that the scaled wake has coherent flow with high magnitude peaks in slipstream velocity due to its clean, periodic nature, as suggested by the larger peaks in the ensemble averages, then the standard deviation would be larger compared to the full-scale wake, with noisier, less coherent flow and thus broader and lower magnitude peaks.

3.6. Gust/TSI

The components processed in calculating the TSI value are shown in Fig. 16. The maximum for each individual run with an equivalent 1 s moving average can be identified, together with the resulting mean and TSI value. In a similar manner to the high variance between runs in the slipstream profiles (Fig. 7), the location and magnitude of the individual maxima are also highly variable, in spite of the significant 1 s moving average applied.

The calculated TSI values for each moving model scenario and for the two full-scale runs for both track-side and platform equivalent positions are presented in Fig. 17. The second full-scale scenario presented is based on runs that would be adequate to process for TSI slipstream holmologation, as outlined in Section 2.5.

At track-side position, the differences between moving model scenarios are not consistent with the unfiltered ensemble averages presented in Fig. 14. The Primary and Reduced Length scenarios TSI values are not significantly different but the Maximum Reynolds

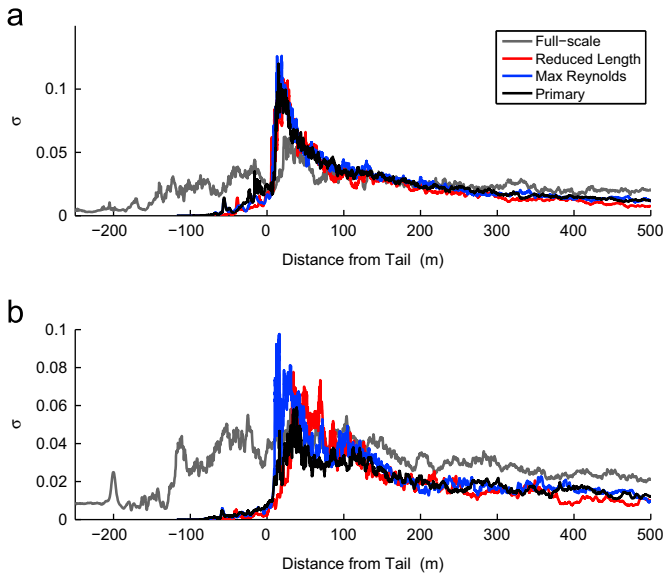

Fig. 15. Ensemble standard deviations. (a) Track-side position and (b) platform position. Black: Primary, blue: Maximum Reynolds, red: Reduced Length scenarios, and grey: full-scale 20 runs with the lowest ambient wind. (For interpretation of the references to colour in this figure caption, the reader is referred to the web version of this article.)

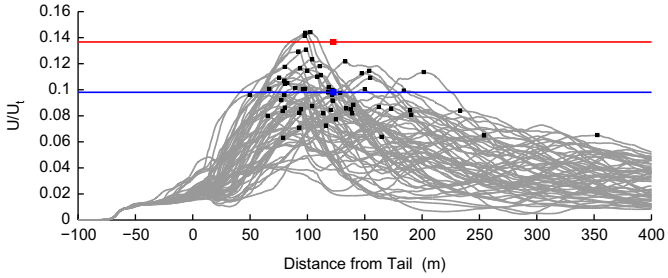

Fig. 16. The components processed to calculate the 'TSI value'. Grey: individual runs with a 1 s equivalent moving average applied, black points: maxima of individual runs with moving average applied, blue point: mean value of maxima, located at mean distance from the tail, and red point: TSI value. Results are taken from track-side measurement position, from the Primary scenario. (For interpretation of the references to colour in this figure caption, the reader is referred to the web version of this article.)

scenario has a larger value. However, the Reduced Length scenario has the largest near-wake peak in the ensemble average, with little difference between the Primary and Maximum Reynolds peaks.

At platform position, the Primary is lower than the other two moving model scenarios, which have the same value. This trend is similar to that found in the near-wake peaks of the ensemble averages in Fig. 14.

The contribution that both the mean and standard deviation makes to the TSI value (Fig. 17) can present a problem with the TSI value's use as a single value comparator. Potentially, different mean values combined with different standard deviations can provide the same TSI value, as seen here in the case of Primary and Reduced Length scenarios at platform equivalent position.

As with the ensemble averages, the moving model results at track-side position compares significantly better to the full scale results than platform position (referring to the low ambient wind full-scale results, which are more ideal, therefore more similar to the moving model set-up). The Maximum Reynolds scenario, the best case scenario, is closest to the low ambient wind full-scale case, with a difference of −1.4%. However, at platform position the difference between the Reduced Length and Maximum Reynolds scenarios to the low ambient wind full-scale is −24%, significantly worse than at track-side. These results are consistent with the moving average profiles in Fig. 14.

When the scaled moving model scenarios are compared to the full-scale results they result in lower TSI values, primarily caused by a smaller contribution from the standard deviation component. This differs to the ensemble standard deviations, where the full-scale results have a lower standard deviation in the near-wake peak. However, the locations of the maxima are not necessarily within the ensemble near-wake peak, as seen in Fig. 16, where there are multiple maxima even beyond 100 m from the tail, where the difference in ensemble standard deviation exists. This highlights the fact that the ensemble mean and standard deviation on their own, or even a superposition of the two, are not necessarily a good representation of gusts. The second full-scale scenario, the selection that conforms to the TSI regulations as outlined in Section 2.5, shows the influence that even a small amount of ambient wind can have on the TSI value through the contribution made when the standard deviation is included.

4. Conclusions

The results from the moving model experiments carried out using an ICE3 model at the TSG facility at DLR Göttingen provided insight into the flow around high-speed trains, specifically their transient wake structure. Although this method only provides individual snapshots of the induced flow, inspection and grouping of individual runs, conditional averaging, and POD processing provide results that agree with previous findings, which have shown that a pair of horizontally oscillating counter-rotating vortices are the dominant feature of the wake. This feature is of considerable interest from the perspective of what causes the slipstream of HSTs as this is where the largest slipstream velocities occur.

Comparing the moving model results to full-scale results was done in an attempt to improve the prediction accuracy for TSI compliance when considering slipstream at early stages in the design phase of trains. The moving model results showed the same 'standard slipstream profile' found in full-scale results; thus, the main flow features captured are expected to be the same between full-scale and scaled experiments.

However, differences did exist between the moving model and full-scale results, with the moving model exhibiting: a closer and narrower near-wake slipstream peak to the tail of the train, and higher peak velocities at track-side, lower at platform position compared to full-scale. The expected cause of these differences is the lower coherence in the wake of the full scale tests caused by the ambient wind and the larger Reynolds number. The difference in the L/H of the two cases could also contribute to a different wake structure.

The ensemble averages indicated that the slipstream profile was partially sensitive to L/H and insensitive to Reynolds number over the range tested. However, the TSI value, based on 'gust' analysis, appeared to be insensitive to L/H and only marginally sensitive to Reynolds number when compared to full-scale results. Analysis of the components of the TSI value highlighted that the TSI can have a similar value despite having different contributions from the mean and standard deviation, this has an effect on its veracity as a single comparative value.

The limitations noted here are often inherent issues of scaled HST aerodynamic experiments. They remain as open questions in the field. The advantages of a moving model method; the correct relative motion between the train-probe and train-ground, and the ability to measure slipstream with reasonable accuracy to which gust analysis can be applied makes it a suitable technique for

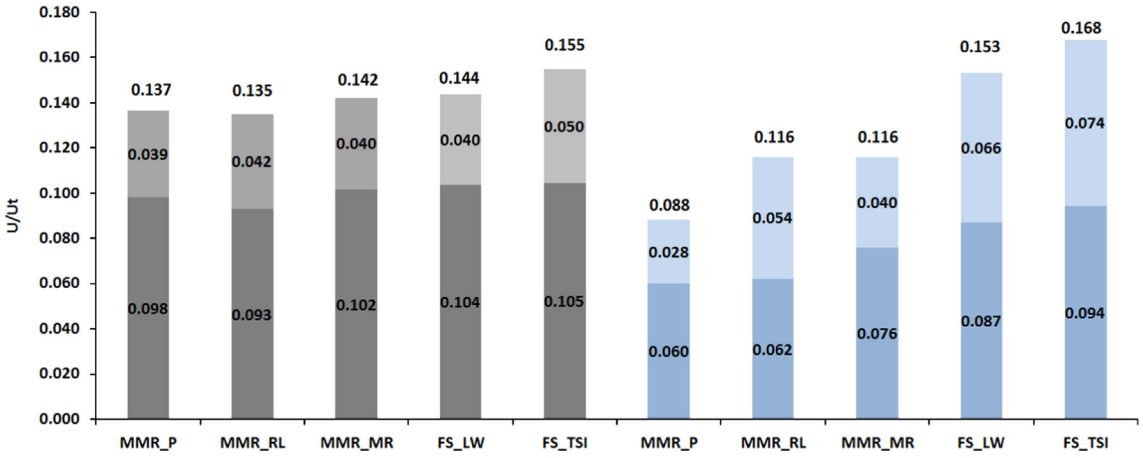

Fig. 17. The 'TSI value': $U+2\sigma$, showing the contribution of its components for track-side (left) and platform (right) positions for the different moving model configurations and two run selection methods of full-scale data. MMR: moving model rig, FS: full-scale, P: Primary scenario, RL: Reduced Length scenario, MR: Maximum Reynolds scenario, LW: 20 lowest ambient wind FS runs, and TSI: FS runs selected using TSI regulations.

assessing TSI-type slipstream risk at the design phase of high-speed trains.

Acknowledgements

The authors wish to acknowledge Dr. K. Ehrenfried (DLR) and Mr. M. Weise, Mr. A. Tietze, Mr. B. Schulz, Mr. U. Gencaslan, Dr. E. Wassen, and Dr. A. Orellano (Bombardier Transportation) for their contributions to this work. Full-scale data presented here is a subset of data measured as a part of Work Package 5 of the EU FP7 AeroTRAIN Project. The Faculty of Engineering, Monash University, is acknowledged for the Engineering Research Living Allowance stipend scholarship for J.R. Bell.

References

Baker, C.J., 2010. The flow around high speed trains. J. Wind Eng. Ind. Aerodyn. 98, 277–298.
Baker, C., 2012. WP5-D5.4 Output Document—Recommendations for TSI Revisions 2012. AeroTRAIN Project Publication, D6.3(1), A.5.1.
Baker, C.J., Dalley, S.J., Johnson, T., Quinn, A., Wright, N.G., 2001. The slipstream and wake of a high-speed train. J. Rail Rapid Transit 215 (2), 83–99.
Baker, C., Quinn, A., Sima, M., Hoefener, L., Licciardello, R., 2012a. Full scale measurement and analysis of train slipstreams and wakes: Part 1. Ensemble averages. Proc. Inst. Mech. Eng. Part F: J. Rail Rapid Transp. 98, 277–298.
Baker, C., Quinn, A., Sima, M., Hoefener, L., Licciardello, R., 2012b. Full scale measurement and analysis of train slipstreams and wakes: Part 2. Gust analysis. Proc. Inst. Mech. Eng. Part F: J. Rail Rapid Transp. 98, 277–298.
Bell, J.R., Burton, D., Thompson, M.C., Herbst, A.H., Sheridan, J., 2014. Wind tunnel analysis of the slipstream and wake of a high-speed train. J. Wind Eng. Ind. Aerodyn. 134, 122–138.
CEN European Standard, 2009. Railway Applications—Aerodynamics—Part 4: Requirements and Test Procedures for Aerodynamics on Open Track, CEN EN 14067-4.
CEN European Standard, 2010. Railway Applications—Aerodynamics—Part 6: Requirements and Test Procedures for Cross Wind Assessment, CEN EN 14067-6.
CEN European Standard, 2013. Railway Applications—Aerodynamics—Part 4: Requirements and Test Procedures for Aerodynamics on Open Track, CEN EN 14067-4.
European Rail Agency (ERA), 2008. EU Technical Specification for Interoperability Relating to the 'Rolling Stock' Sub-System of the Trans-European High-Speed Rail System (HS RST TSI), 232/EC.
Gilbert, T., Baker, C.J., Quinn, A., 2013. Gusts caused by high-speed trains in confined spaces and tunnels. J. Wind Eng. Ind. Aerodyn. 121, 39–48.
Graftieaux, L., Michard, M., Grosjean, N., 2001. Combining piv, pod and vortex identification algorithms for the study of unsteady turbulent swirling flows. Meas. Sci. Technol. 12, 1422–1429.
Heine, D., Lauenroth, G., Haff, J., Huntgeburth, S., Ehrenfried, K., 2013. High-speed particle image velocimetry on a moving train model. In: 2nd International Symposium on Rail Aerodynamics, Berlin, Germany.
Hemida, H., Baker, C.J., Gao, G., 2013. The calculation of train slipstreams using large-eddy simulation. Proc. Inst. Mech. Eng. Part F: J. Rail Rapid Transp. 228, 25–36.
Huang, S., Hemida, H., Yang, M., 2014. Numerical calculation of the slipstream generated by a crh2 high-speed train. Proc. Inst. Mech. Eng. Part F: J. Rail Rapid Transp., http://dx.doi.org/10.1177/0954409714528891.
Morel, T., 1980. Effect of base slant on flow in the near wake of an axisymmetric cylinder. Aeronaut. Q., 132–147.
Muld, T., Efraimsson, G., Hennigson, D.S., 2012a. Flow structures around a high-speed train extracted using proper orthogonal decomposition and dynamic mode decomposition. J. Rail Rapid Transit 57, 87–97.
Muld, T., Efraimsson, G., Hennigson, D.S., 2012b. Mode decomposition on surface-mounted cube. Flow Turbul. Combust. 88, 279–310.
Muld, T., Efraimsson, G., Hennigson, D.S., 2014a. Mode decomposition and slipstream velocities in the wake of two high-speed trains. Proc. Inst. Mech. Eng. Part F: J. Rail Rapid Transp. accepted for publication.
Muld, T., Efraimsson, G., Hennigson, D.S., 2014b. Wake characteristics of high-speed trains with different lengths. Proc. Inst. Mech. Eng. Part F: J. Rail Rapid Transit 228 (4), 333–342.
Munson, B.R., Young, D.F., Okiishi, T.H., 2006. Fundamentals of Fluid Mechanics, 5th ed. John Wiley and Sons, Hoboken, New Jersey, USA.
Perrin, R., Braza, M., Cid, E., Cazin, S., Barthet, A., Sevrain, A., Mockett, C., Thiele, F., 2007. Obtaining phase averaged turbulence properties in the near wake of a circular cylinder at high Reynolds number using pod. Exp. Fluids 43, 341–355.
Pii, L., Vanoli, E., Polidoro, F., Gautier, S., Tabbal, A., 2014. Full scale simulation of a high speed train for slipstream prediction. In: Proceedings of the Transport Research Arena, Paris, France.
Pope, C.W., 2007. Effective Management of Risk from Slipstream Effects at Trackside and Platforms. Rail Safety and Standards Board—T425 Report.
Schulte-Werning, B., Heine, B., Matschke, C., 2001. Slipstream development and wake flow characteristics of modern high-speed trains. J. Appl. Math. Mech. 81 (S3), 789–790.
Schulte-Werning, B., Heine, B., Matschke, C., 2003. Unsteady wake flow characteristics of high-speed trains. Proc. Appl. Math. Mech. 2, 332–333.
Sterling, M., Baker, C.J., Jordan, S.C., Johnson, T., 2008. A study of the slipstreams of high-speed passenger trains and freight trains. Proc. Inst. Mech. Eng. Part F: J. Rail Rapid Transp. 222, 177–193.
Weise, M., Schober, M., Orellano, A., 2006. Slipstream velocities induced by trains. In: Proceedings of the WSEAS International Conference on Fluid Mechanics and Aerodynamics, Elounda, Greece.
Yao, S., Sun, Z., Guo, D., Chen, D., Yang, G., 2013. Numerical study on wake characteristics of high-speed trains. Acta Mech. Sin. 29 (6), 811–822.